Published for SISSA by Springer

Received: May 6, 2025
Accepted: June 10, 2025
Published: July 9, 2025

Observation of the decay $B_s^0 \to K^0 p\bar{p}$ and measurement of the $B_{(s)}^0 \to K^0 p\bar{p}$ branching fractions

The LHCb collaboration

E-mail: duanqing.liu@cern.ch

Abstract: A study of the charmless baryonic decays $B_{(s)}^0 \to K^0 p\bar{p}$ is presented, where $B_{(s)}^0$ denotes either a B^0 or a B_s^0 meson. The analysis is based on proton-proton collision data collected by the LHCb experiment at centre-of-mass energies of 7, 8, and 13 TeV, corresponding to an integrated luminosity of $9\,\text{fb}^{-1}$. The decay $B_s^0 \to K^0 p\bar{p}$ is observed for the first time, with a measured branching fraction of $(9.14 \pm 1.69 \pm 0.90 \pm 0.33 \pm 0.20) \times 10^{-7}$ and a significance of 5.6σ. The uncertainties respectively account for statistical and systematic contributions, the precision of the branching fraction of the normalisation channel $B^0 \to K^0\pi^+\pi^-$ and the fragmentation fraction ratio f_s/f_d. The branching fraction determined for $B^0 \to K^0 p\bar{p}$ is $(2.82 \pm 0.08 \pm 0.12 \pm 0.10) \times 10^{-6}$, which is the most precise measurement to date.

Keywords: B Physics, Branching fraction, Flavour Physics, Hadron-Hadron Scattering

ArXiv ePrint: 2504.21269

https://doi.org/10.1007/JHEP07(2025)121

JHEP07(2025)121

Contents

1 Introduction 1

2 Detector and simulation 2

3 Event selection 3

4 Signal extraction 4

5 Branching fraction measurement 5

6 Systematic uncertainties 7

7 Results and conclusion 9

A Fit results of all subsamples 11

The LHCb collaboration 17

1 Introduction

The $B^0_{(s)} \to K^0 p\overline{p}$ decays involve contributions from both QCD penguin and tree-level amplitudes. The QCD penguin contributions proceed via the $b \to q\overline{q}s$ and $b \to q\overline{q}d$ quark transitions (where $q = u, d$), while the tree-level $b \to u$ contributions are CKM suppressed [1]. These processes provide a valuable probe into the dynamics of charmless B meson decays. The $p\overline{p}$ mass distribution that peaks near threshold in these decays is a key feature indicating the involvement of nontrivial intermediate states that influence the decay dynamics. The observed decay rate hierarchy, where the $B^0 \to K^0 p\overline{p}$ rate is significantly lower than that of the $B^+ \to K^+ p\overline{p}$ mode, contrasts with other decay modes such as $B^{0,+} \to \pi^0 K^{0,+}$ and $B^{0,+} \to J/\psi K^{0,+}$ [2–7].

Measurements of branching fractions and CP asymmetries are essential for testing and refining theoretical model [8, 9]. The relative branching fractions of $B^0 \to K^0 p\overline{p}$ and $B^0_s \to K^0 p\overline{p}$ decays provide precise tests of flavour symmetries, as their quark-level diagrams are related not only through the interchange of d and s spectator quarks but also through modifications to the weak decay process to ensure the correct final-state quark content. Additionally, these decays serve as key observables for studying CP violation in loop-dominated processes [10]. Time-dependent Dalitz analyses can measure CP-violating parameters, which may be sensitive to potential physics beyond the Standard Model [11, 12].

In this paper, a search for the $B^0_s \to K^0 p\overline{p}$ decay mode is performed, and the branching fractions of $B^0_{(s)} \to K^0 p\overline{p}$ decays are determined by employing the well-known $B^0 \to K^0 \pi^+ \pi^-$ decays for normalisation [13]. In both decays, the K^0 is reconstructed through the two-pion decay of its short-lived mass eigenstate ($K^0_S \to \pi^+ \pi^-$). This analysis uses the full Run 1 (2011–2012) and Run 2 (2015–2018) LHCb data samples of proton-proton (pp) collisions at

JHEP07(2025)121

centre-of-mass energies of 7, 8, and 13 TeV, corresponding to an integrated luminosity of about $9\,\text{fb}^{-1}$. To improve statistical significance, the data sample is divided into four subsamples (2011, 2012, 2015–2016, and 2017–2018) based on variations in peak shapes, which arise from differences in the centre-of-mass energies and trigger configurations during data collection.

While the measured $p\bar{p}$ and K^0p mass regions span the full kinematic range, contributions from charmonium (η_c, J/ψ, $\psi(2S)$) and open-charm (Λ_c^+) decays are explicitly excluded from the respective regions. A dedicated efficiency correction accounts for the phase-space contribution in the excluded regions, ensuring that the aforementioned mass vetoes have a negligible impact on the branching fraction measurement. The $B^0 \to K^0 p\bar{p}$ branching fractions have been measured by the BaBar and Belle collaborations [7, 14], with both results in good agreement. These previous measurements also cover the full $p\bar{p}$ kinematic range, allowing a direct comparison.

2 Detector and simulation

The LHCb detector [15, 16] is a single-arm forward spectrometer covering the pseudorapidity range $2 < \eta < 5$, designed for the study of particles containing b or c quarks. The detector includes a high-precision tracking system consisting of a silicon-strip vertex detector surrounding the pp interaction region [17], a large-area silicon-strip detector located upstream of a dipole magnet with a bending power of about 4 T m, and three stations of silicon-strip detectors and straw drift tubes [18] placed downstream of the magnet. The tracking system provides a measurement of momentum, p, of charged particles with a relative uncertainty that varies from 0.5% at low momentum to 1.0% at 200 GeV/c. The minimum distance of a track to a primary vertex (PV), the impact parameter (IP), is measured with a resolution of $(15 + 29/p_{\text{T}})$ µm, where p_{T} is the component of the momentum transverse to the beam, in GeV/c. Different types of charged hadrons are distinguished using information from two ring-imaging Cherenkov detectors [19]. Photons, electrons and hadrons are identified by a calorimeter system consisting of scintillating-pad and preshower detectors, an electromagnetic calorimeter and a hadronic calorimeter. Muons are identified by a system composed of alternating layers of iron and multiwire proportional chambers [20].

Simulation is used to model the effects of detector acceptance and selection requirements, as well as to study backgrounds from other b-hadron decays. Both the signal and normalisation decays are simulated using a phase-space model. In the simulation, pp collisions are generated using Pythia with a specific LHCb configuration [21]. Decays of unstable particles are described by EvtGen [22], in which final-state radiation is generated using Photos [23]. The interaction of the generated particles with the detector, and its response, are implemented using the Geant4 toolkit [24, 25] as described in ref. [26].

The online event selection is performed by a trigger [27], which consists of a hardware stage, based on information from the calorimeter and muon systems, followed by a software stage, which applies a full event reconstruction. At the hardware trigger level, events are required to have a muon with high p_{T} or a hadron, photon or electron with high transverse energy in the calorimeters. The software trigger requires a two-, three- or four-track secondary vertex with a significant primary pp interaction vertices with PVs. At least one charged particle must have high transverse momentum and be inconsistent with originating from any

JHEP07(2025)121

reconstructed PV. A multivariate algorithm [28, 29] is used for the identification of secondary vertices consistent with the decay of a b hadron. It is required that the software trigger decision must have been caused by tracks from the decay of the signal B candidate.

3 Event selection

To suppress background, events satisfying the hardware and software trigger requirements undergo an additional two-stage offline selection: a loose preselection followed by a multivariate selection. The loose preselection, which primarily relies on topological features to distinguish signal from background, includes criteria such as the displacement of the B decay products from the PV.

Reconstructed $K^0_S \to \pi^+\pi^-$ decays are classified into two categories: the 'long' category, which includes K^0_S mesons that decay at shorter flight distances, allowing pion tracks to be reconstructed in the vertex detector, and the 'downstream' category, which comprises K^0_S mesons that decay further downstream, where the pion track segments cannot be formed in the vertex detector. The long category has better mass, momentum and vertex resolution than the downstream category. The K^0_S candidates are formed by combining two charged pions associated with long (downstream) tracks, with momenta greater than 2 GeV/c (6 GeV/c), and inconsistent with originating from a PV; the dipion vertex fit must be of good quality, and the resulting invariant mass must lie within ± 20 MeV/c (± 30 MeV/c) of the known K^0_S mass [13]. The K^0_S vertex must be significantly displaced from its associated PV, which is defined using the difference in the vertex-fit χ^2 of a given PV reconstructed with and without the K^0_S candidate.

The B candidates are formed by combining a K^0_S candidate with two oppositely charged hadrons, either $p\overline{p}$ or $\pi^+\pi^-$. In the former case, to ensure good particle identification (PID), the proton momentum is required to be within $8 < p < 100$ GeV/c for Run 1 and $11 < p < 100$ GeV/c for Run 2 [30]. The scalar sum of the transverse momenta of the K^0_S meson and two proton candidates must be greater than 3.0 GeV/c (4.2 GeV/c), for long (downstream) candidates, and at least two of these three decay products must have $p_T > 0.8$ GeV/c. The reconstructed B candidate vertex is required to be of good quality, significantly separated from any PV, and isolated from other tracks. The B candidates should also be consistent with originating from a PV. Finally, the K^0_S decay vertex is required to be at least 30 mm downstream of the B vertex along the beam direction. The PID requirements are applied to ensure each final-state particle is consistent with its hypothesis.

A boosted decision tree (BDT) classifier [31, 32], implemented in the TMVA toolkit [33], is used to separate signal from background. The classifier is trained using variables related to the B candidate, such as p_T, pseudorapidity, decay time, the vertex-fit quality, and the angle between its reconstructed momentum and flight direction. It also considers vertex properties such as the consistency with the PV, the separation between the B and K^0_S vertices along the beam direction, and the impact parameter significance and p_T of the final-state particles.

As the decay topologies of $B^0_{(s)} \to K^0_S p\overline{p}$ and $B^0 \to K^0_S \pi^+\pi^-$ are nearly identical, only $B^0 \to K^0_S p\overline{p}$ decay samples are used to train the classifier. The signal training sample consists of simulated $B^0 \to K^0_S p\overline{p}$ decays, while the background training sample consists of data from the upper-mass sideband region, defined as $5450 < m(K^0_S p\overline{p}) < 5800$ MeV/c^2.

JHEP07(2025)121

The $B^0_{(s)} \to K^0_S p\bar{p}$ and $B^0 \to K^0_S \pi^+\pi^-$ candidates are categorised by K^0_S reconstruction type (long and downstream) and data-taking period (2011 and 2012 share a common selection). Selections are optimised separately for the $B^0 \to K^0_S p\bar{p}$ branching fraction measurement and the $B^0_s \to K^0_S p\bar{p}$ search, with the BDT requirement optimised independently for each subsample. For the previously established $B^0 \to K^0_S h^+h^-$ decays, with h=π or p, the BDT selection is optimised for signal significance, defined as $N_{\rm sig}/\sqrt{N_{\rm sig}+N_{\rm bkg}}$, where $N_{\rm sig}$ and $N_{\rm bkg}$ represent the numbers of expected signal and background candidates within the signal $5234 < m(K^0_S h^+h^-) < 5324\,\text{MeV}/c^2$. The value of $N_{\rm sig}$ is estimated using the signal yield extracted from fits to data selected with a looser BDT selection requirement and scaling it by the efficiency of the tighter BDT selection, as determined from simulation. The value of $N_{\rm bkg}$ is calculated by fitting the upper mass sideband region and extrapolating into the signal region. In contrast, since the $B^0_s \to K^0_S p\bar{p}$ decay mode has not yet been observed, the BDT selection is optimised to enhance its sensitivity, based on the figure-of-merit $\varepsilon_{\rm sig}/(\alpha/2+\sqrt{N_{\rm bkg}})$ [34], where $\varepsilon_{\rm sig}$ is the signal efficiency, estimated from simulation, and $\alpha = 5$ is the desired significance for the signal channel.

After the selection process, the background includes B decays with similar or identical final states that proceed through intermediate open-charm or charmonium states. Dedicated invariant-mass vetoes around the known mass values [13] are applied to reject these backgrounds. Specifically, the veto windows are set to $\pm 30\,\text{MeV}/c^2$ for the Λ_c^+ baryon, $\pm 45\,\text{MeV}/c^2$ for the η_c state, $\pm 25\,\text{MeV}/c^2$ for the J/ψ state, and $\pm 35\,\text{MeV}/c^2$ for the $\psi(2S)$ state. These ranges typically correspond to $\pm 3\sigma$, where σ is the mass resolution of the considered resonance. The effect of the vetoes is determined using simulations, which account for the exclusion of the $p\bar{p}$ and $K^0_S p$ regions.

4 Signal extraction

An unbinned maximum-likelihood fit to the invariant mass is performed for each of the eight subsamples; the invariant masses are determined by constraining the K^0_S mass to its known value [13]. The 2011 and 2012 data share the candidate selection but have separate mass fits and efficiency calculations due to variations in peak shapes, within the mass regions $5000 < m(K^0_S p\bar{p}) < 5600\,\text{MeV}/c^2$ for $B^0 \to K^0_S p\bar{p}$ and $5050 < m(K^0_S \pi^+\pi^-) < 5600\,\text{MeV}/c^2$ for $B^0 \to K^0_S \pi^+\pi^-$. For the sample optimised for the $B^0_s \to K^0_S p\bar{p}$ search, the fit is performed within the mass range $5000 < m(K^0_S p\bar{p}) < 5600\,\text{MeV}/c^2$ on two subsamples, categorised by the K^0_S reconstruction type. While separate event selections are applied to the 2011–2012, 2015–2016, and 2017–2018 datasets, they share the same mass fits and efficiency calculations.

For both the $B^0_{(s)} \to K^0_S p\bar{p}$ and the normalisation channel $B^0 \to K^0_S \pi^+\pi^-$ decays, the fit model includes components for the signal, partially reconstructed background, and combinatorial background. The probability density function for the B^0 and B^0_s signal peaks consists of two double-sided Crystal Ball (DSCB) functions [35]. In the fit, the B^0 peak position and $B^0_{(s)}$ mass resolution are allowed to vary freely, while the B^0_s peak position is constrained as $\mu(B^0_s) = \mu(B^0) + \Delta m$, with $\Delta m = 87.26\,\text{MeV}/c^2$ being the known mass difference between the B^0 and B^0_s mesons [13]. The tail parameters of the DSCB functions for B^0 and B^0_s are fixed to values obtained from their respective simulations.

JHEP07(2025)121

The partially reconstructed background arises from b-hadron decays into final states containing $K^0_S h^+ h^-$ (where $h = \pi, p$) along with at least one unreconstructed particle. As a result, its invariant-mass distribution has a broad shape, peaking at values lower than the parent b-hadron mass. Its shape is modelled using an ARGUS function convolved with a Gaussian function [36], where the curvature of the ARGUS function is fixed, while the slope, the threshold, and the Gaussian mean and width parameters are allowed to vary. The combinatorial background component, arising from combinations of unrelated particles, is modelled by an exponential function, with slope parameter allowed to vary.

Background contributions from b-hadron decays that have a topology similar to the signal channel, but where final-state hadrons (π^+ or K^+) are misidentified, are also considered in the fits. The contribution from double misidentification is found to be negligible due to its small yield, and therefore only the singly misidentified components are included in the fit to the normalisation mode $B^0 \to K^0_S \pi^+ \pi^-$. These components are modelled using a DSCB function, with the tail parameters fixed from simulation, while the peak position and width are allowed to vary. In the fit, the $B^0_{(s)} \to K^0_S K^\pm \pi^\mp$ yield is constrained to the yield of the $B^0 \to K^0_S \pi^+ \pi^-$ decays with a fraction that incorporates the known branching fraction ratio, the efficiency ratio from simulation, and the misidentification rates measured in data control samples.

The individual fits of subsamples are presented in appendix A. The sum of signal yields from the individual fits are $1\,791 \pm 52$ for $B^0 \to K^0_S p\overline{p}$ and $32\,145 \pm 230$ for $B^0 \to K^0_S \pi^+ \pi^-$. A peaking structure is observed in the $m(K^0_S p\overline{p})$ distribution near the known B^0_s meson mass. The sum of the signal yields, determined using the selection criteria optimised for the $B^0_s \to K^0_S p\overline{p}$ search, is 66 ± 12. Based on statistical uncertainty alone, the signal significance is 7.1σ, as calculated using Wilks' theorem [37]. When systematic uncertainties are also taken into account, the significance decreases to 5.6σ, as discussed in section 7. For visualisation, the fit results for the full dataset are shown in figure 1.

5 Branching fraction measurement

The branching fraction of $B^0_{(s)} \to K^0_S p\overline{p}$ decays is determined relative to the normalisation channel $B^0 \to K^0_S \pi^+ \pi^-$ through the ratio

$$\frac{\mathcal{B}(B^0_{(s)} \to K^0_S p\overline{p})}{\mathcal{B}(B^0 \to K^0_S \pi^+ \pi^-)} = \frac{\varepsilon^{\text{sel}}(B^0 \to K^0_S \pi^+ \pi^-)}{\varepsilon^{\text{sel}}(B^0_{(s)} \to K^0_S p\overline{p})} \times \frac{N(B^0_{(s)} \to K^0_S p\overline{p})}{N(B^0 \to K^0_S \pi^+ \pi^-)} \times \frac{f_d}{f_{d(s)}}, \tag{5.1}$$

where $\varepsilon^{\text{sel}}(X)$ and $N(X)$ are the efficiencies and yields of the different channels, X, and f_d and f_s are the hadronisation fractions of a b quark into a B^0 or B^0_s meson, respectively. The efficiency term includes the effects of geometrical acceptance and trigger, reconstruction and selection; it is determined using simulation and dedicated calibration procedures. The ratio f_s/f_d has been measured by the LHCb experiment, using hadronic and semileptonic decays at different centre-of-mass energies [38]. Taking into account the integrated luminosity and the production cross-section at each centre-of-mass energy, a weighted average value of 0.2486 ± 0.0078 is obtained.

Three-body hadronic decays, such as $B^0_{(s)} \to K^0_S h^+ h^-$, exhibit a complex phase-space structure that can be visualised in a Dalitz plot [39]. The decay amplitude can be influenced

JHEP07(2025)121

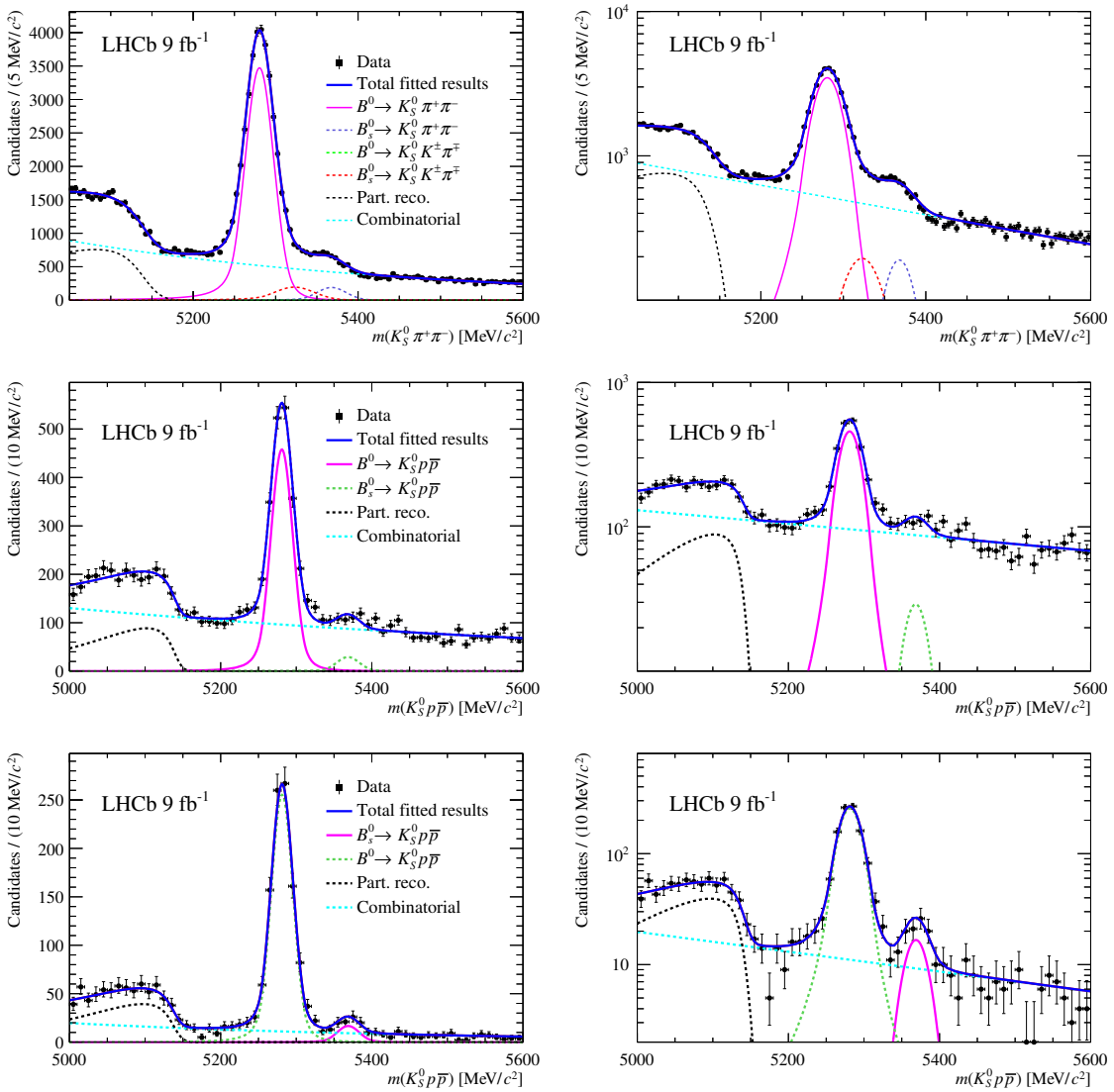

Figure 1. Invariant-mass distributions of $K^0_S h^+h^-$ candidates that pass all selection criteria, combining all subsamples, are shown (left) on a linear scale and (right) on a logarithmic scale. Each row corresponds to a given decay mode: (top) $B^0 \to K^0_S\pi^+\pi^-$, (middle) $B^0 \to K^0_S p\bar{p}$, (bottom) $B^0_s \to K^0_S p\bar{p}$. Fit results are also shown.

by intermediate quasi-two-body resonances and broad, nonresonant contributions that overlap and interfere. This nonuniform distribution of events typically results in higher probability densities near the kinematic boundaries of the Dalitz plot. The overall efficiency of the reconstruction and selection depends on the Dalitz structure of the decay. To simplify the description of the phase space, and to avoid edge effects, the Dalitz plot is transformed into a square representation [40]. This transformation ensures a more uniform distribution of candidates near the kinematic boundaries, where resonances are concentrated and efficiency variations are significant. Along with this transformation, the simulation is weighted to match the data. Background-subtracted Dalitz plots are obtained using the *sPlot* method [41],

JHEP07(2025)121

where each candidate is assigned a weight derived from fits to the $m(K^0_S p\bar{p})$ and $m(K^0_S\pi^+\pi^-)$ distributions in section 4. The selection efficiency is then corrected using signal weights from data and the per-event efficiency from weighted simulation, giving

$$\varepsilon^{\text{sel}} = \frac{\sum_e W_e}{\sum_e \frac{W_e}{\varepsilon_{e(j)}}}, \tag{5.2}$$

where W_e is the signal weight associated with the candidate e and $\varepsilon_{e(j)}$ its efficiency, taken from the corresponding bin j in the square Dalitz plot, which is split into a uniform 5×5 grid. The value of $\varepsilon_{e(j)}$ varies in the range 0.001–0.005 for $B^0 \to K^0_S p\bar{p}$, 0.001–0.003 for $B^0 \to K^0_S\pi^+\pi^-$ and 0.0003–0.0013 for $B^0_s \to K^0_S p\bar{p}$ decays, with a smooth and well-controlled overall behaviour.

The PID efficiencies and misidentification rates are derived from simulations based on the kinematic properties of the tracks in the decay process. These are then corrected, exploiting the PID response in calibration data. A weighting procedure is performed in bins of momentum, pseudorapidity, and event multiplicity, accounting for kinematic correlations between the tracks [42]. Differences in tracking efficiency are corrected as a function of the track momentum and pseudorapidity using data control channels. Differences in hardware trigger response between data and simulation are determined using calibration samples of $D^{*+} \to D^0(\to K^-\pi^+)\pi^+$ and $\Lambda \to p\pi^-$ decays where the trigger requirement is satisfied independently of the decay products. The trigger response is analysed based on the hadron charge, p_{T}, calorimeter region, and cluster overlap of final-state particles from signal decays, with a correction for the average underlying energy, which includes contributions from multiple interactions and diffuse energy deposits [27, 43, 44].

The efficiency correction due to mass vetoes is estimated using simulation, which implements a uniform phase-space decay model. Therefore, the measured results can be directly compared with those from other experiments, which are determined across the entire $p\bar{p}$ mass range. Finally, the efficiency ratio between $B^0 \to K^0_S\pi^+\pi^-$ and $B^0 \to K^0_S p\bar{p}$ decays is 1.02 ± 0.02, while that between $B^0 \to K^0_S\pi^+\pi^-$ and $B^0_s \to K^0_S p\bar{p}$ decays is 2.23 ± 0.12. The significantly larger ratio observed in the latter case is primarily attributed to differences in the selection criteria, with the most notable contribution arising from the distinct BDT requirements applied to the three decay modes. The uncertainties stem from the limited size of the signal simulation. These efficiency ratios are calculated by combining the values determined on each data sample.

6 Systematic uncertainties

The $B^0_{(s)} \to K^0_S p\bar{p}$ branching fractions are measured relative to the decay $B^0 \to K^0_S\pi^+\pi^-$, as expressed in eq. (5.1). Since similar selections and fit procedures are used for decays in the numerator and denominator, several potential systematic effects are expected to cancel in the ratio. The remaining uncertainties are discussed in this section and categorised based on their influence on either the yield measurements (N) or the efficiency (ε^{sel}). The uncertainty on f_s/f_d is also included where appropriate. The total, statistical and systematic uncertainties are summarised in table 1.

JHEP07(2025)121

The systematic uncertainty associated with the choice of fit model is evaluated by comparing signal yields obtained from the baseline and alternative fit models, with variations applied to the signal, partially reconstructed, misidentified, and combinatorial background components. The difference in signal yields between the two models is fitted with a Gaussian function, and the systematic uncertainty is taken as the quadrature sum of the Gaussian mean and width.

For each alternative model, one fit component is varied at a time. For the signal and misidentified background models, the baseline DSCB functions are replaced with a sum of a Student's t-distribution and a Gaussian function. The exponential function modelling the combinatorial background is replaced by a second-order Chebyshev polynomial function. To estimate the impact of partially reconstructed background, the fit is performed in the restricted invariant-mass range of 5150–5600 MeV/c^2, where its contribution is reduced.

The accuracy of the efficiency determination is limited by the size of the signal simulation samples, which is propagated as a systematic uncertainty. Additionally, the effect of the choice of binning scheme used to subdivide the square Dalitz plot is estimated based on the spread of the average efficiencies determined from various alternative binning schemes.

The procedure to evaluate the efficiencies of the PID requirements, described in section 4, uses calibration tracks that systematically differ from the signal tracks. While the binning procedure attempts to mitigate these differences, there could be some remaining systematic effect. This is addressed by considering different ensembles of kinematical binning schemes to determine the efficiency. An overall 1% systematic uncertainty is assigned to quantify any bias due to the procedure and is added in quadrature with the statistical uncertainties originating from the finite size of the simulation samples. A relative systematic uncertainty on the tracking corrections is assigned for the data-taking periods of Run 1 and Run 2, accounting for differences in hadronic interactions of protons and pions with the detector material [45].

Possible sources of systematic uncertainty related to the efficiency estimation of the hardware trigger have been studied. Two sources are identified: one arising from the imperfect simulation of the rate at which overlapping tracks in the hadron calorimeter merge into a single hadron trigger candidate, and the other from the choice of the data calibration sample. The first uncertainty is evaluated as the difference in the trigger efficiency correction with and without the overlapping cluster corrections. For the second, correction factors are determined using a sample of reconstructed $B^0 \to J/\psi K^+\pi^-$ decays, and the difference between the factors obtained from the two calibration samples is assigned as the systematic uncertainty. These two uncertainties are treated as independent and are summed in quadrature to obtain the total systematic uncertainty associated with the hardware trigger efficiency. The differences observed between the $B^0 \to K^0_S p\overline{p}$ and $B^0_s \to K^0_S p\overline{p}$ channels are attributed to the limited sample size and to possible residual double counting effects, which are expected to be small.

The uncertainty associated with the BDT selection is evaluated by varying the requirement and recalculating the efficiency and yields. The resulting deviation in the branching fractions is assigned as an uncertainty. Similarly, the uncertainty from the choice of mass veto regions, used to exclude charm and charmonium contributions, is assessed by varying their size and evaluating the selection performance again. The resulting changes are used to determine the deviation in the branching fractions, which is assigned as the corresponding uncertainty.

JHEP07(2025)121

	$\frac{\mathcal{B}(B^0\to K^0_S p\bar{p})}{\mathcal{B}(B^0\to K^0_S\pi^+\pi^-)}$	$\frac{\mathcal{B}(B^0_s\to K^0_S p\bar{p})}{\mathcal{B}(B^0\to K^0_S\pi^+\pi^-)}$
Statistical	3.0%	18.4%
Fit model	1.0%	4.7%
Simulation sample size	1.7%	5.5%
Binning	2.4%	2.6%
PID	1.1%	1.2%
Tracking	0.5%	0.5%
L0 trigger	3.6%	5.5%
BDT selection	0.9%	1.2%
Mass veto	0.7%	1.8%
B^0_s lifetime	—	3.1%
Total systematic	5.0%	9.8%
f_s/f_d	—	2.2%

Table 1. Summary of the relative statistical and systematic uncertainties on the branching fraction ratios, expressed in percent. The total systematic uncertainty represents the quadrature sum of all individual systematic contributions.

It is important to note that the efficiency is evaluated over the full range of the $p\bar{p}$ and $K^0_S p$ invariant masses. While the vetoed regions do contain a small amount of signal, they represent only a tiny portion of the phase space. As a result, excluding these regions has a minimal effect on the overall efficiency and the final results.

The uncertainty in the B^0 and B^0_s lifetimes affects the selection efficiency. For $B^0\to K^0_S p\bar{p}$ and $B^0\to K^0_S\pi^+\pi^-$ decays, the effect on the ratio of branching fractions is negligible. The width difference between the B^0_{sH} and B^0_{sL} states leads to a lifetime variation of up to 5% [13, 46]. Following ref. [47], the systematic uncertainty is evaluated by weighting the default $B^0_s\to K^0_S p\bar{p}$ decay time distribution and comparing it to variations of $\pm5\%$. The resulting maximum deviation in the B^0_s efficiency is quoted in table 1.

The systematic uncertainties are combined while accounting for their correlations. The correlation coefficients are 0% for the sample size and mass veto systematics, 50% for the fit model, PID, binning, tracking, and L0 trigger systematics, and 100% for the BDT selection. The 'L0 Trigger' uncertainty is the dominant contribution.

7 Results and conclusion

A search for the $B^0_s\to K^0_S p\bar{p}$ decay and measurements of the branching fraction ratios of $B^0_{(s)}\to K^0_S p\bar{p}$ decays are performed, using a pp collision data sample recorded with the LHCb detector from 2011 to 2018, corresponding to an integrated luminosity of $9\,\text{fb}^{-1}$. The decay $B^0_s\to K^0_S p\bar{p}$ is observed for the first time, with a significance of 5.6 standard deviations, including both statistical and systematic uncertainties.

JHEP07(2025)121

The branching fractions of the two decay modes are measured relative to the $B^0 \to K^0_S \pi^+\pi^-$ decay. The branching fraction ratios are determined independently for two K^0_S reconstruction categories and different data-taking periods for $B^0 \to K^0_S p\bar{p}$, and found to be consistent between all subsamples. Combining these results using the Best Linear Unbiased Estimate method [48], which takes into account the correlations of systematic uncertainties among different subsamples, yields:

$$\frac{\mathcal{B}(B^0 \to K^0_S p\bar{p})}{\mathcal{B}(B^0 \to K^0_S \pi^+\pi^-)} = (5.67 \pm 0.17 \pm 0.28) \times 10^{-2},$$
$$\frac{\mathcal{B}(B^0_s \to K^0_S p\bar{p})}{\mathcal{B}(B^0 \to K^0_S \pi^+\pi^-)} = (1.84 \pm 0.34 \pm 0.18 \pm 0.04) \times 10^{-2},$$
$$\frac{\mathcal{B}(B^0_s \to K^0_S p\bar{p})}{\mathcal{B}(B^0 \to K^0_S p\bar{p})} = (3.25 \pm 0.61 \pm 0.36 \pm 0.07) \times 10^{-1},$$

where the first uncertainty is statistical, the second systematic in each case, and the third originates from the ratio of fragmentation fractions of the B^0_s and B^0 mesons, f_s/f_d. Using the known branching fraction of the normalisation channel, $\mathcal{B}(B^0 \to K^0\pi^+\pi^-) = (4.97 \pm 0.18) \times 10^{-5}$ [13], the absolute branching fractions of $B^0 \to K^0 p\bar{p}$ and $B^0_s \to K^0 p\bar{p}$ decays are determined to be

$$\mathcal{B}(B^0 \to K^0 p\bar{p}) = (2.82 \pm 0.08 \pm 0.12 \pm 0.10) \times 10^{-6},$$
$$\mathcal{B}(B^0_s \to K^0 p\bar{p}) = (9.14 \pm 1.69 \pm 0.90 \pm 0.33 \pm 0.20) \times 10^{-7},$$

where the third and fourth uncertainties are due to the uncertainties of the branching fraction of the normalisation channel, and f_s/f_d, respectively. The measured $B^0 \to K^0 p\bar{p}$ branching fraction is consistent with and more precise than the world average value $(2.66 \pm 0.32) \times 10^{-6}$ [13].

Acknowledgments

We express our gratitude to our colleagues in the CERN accelerator departments for the excellent performance of the LHC. We thank the technical and administrative staff at the LHCb institutes. We acknowledge support from CERN and from the national agencies: ARC (Australia); CAPES, CNPq, FAPERJ and FINEP (Brazil); MOST and NSFC (China); CNRS/IN2P3 (France); BMBF, DFG and MPG (Germany); INFN (Italy); NWO (Netherlands); MNiSW and NCN (Poland); MCID/IFA (Romania); MICIU and AEI (Spain); SNSF and SER (Switzerland); NASU (Ukraine); STFC (United Kingdom); DOE NP and NSF (U.S.A.). We acknowledge the computing resources that are provided by ARDC (Australia), CBPF (Brazil), CERN, IHEP and LZU (China), IN2P3 (France), KIT and DESY (Germany), INFN (Italy), SURF (Netherlands), Polish WLCG (Poland), IFIN-HH (Romania), PIC (Spain), CSCS (Switzerland), and GridPP (United Kingdom). We are indebted to the communities behind the multiple open-source software packages on which we depend. Individual groups or members have received support from Key Research Program of Frontier Sciences of CAS, CAS PIFI, CAS CCEPP, Fundamental Research Funds for the Central Universities, and Sci. & Tech. Program of Guangzhou (China); Minciencias (Colombia); EPLANET, Marie Skłodowska-Curie Actions, ERC and NextGenerationEU (European Union); A*MIDEX, ANR,

JHEP07(2025)121

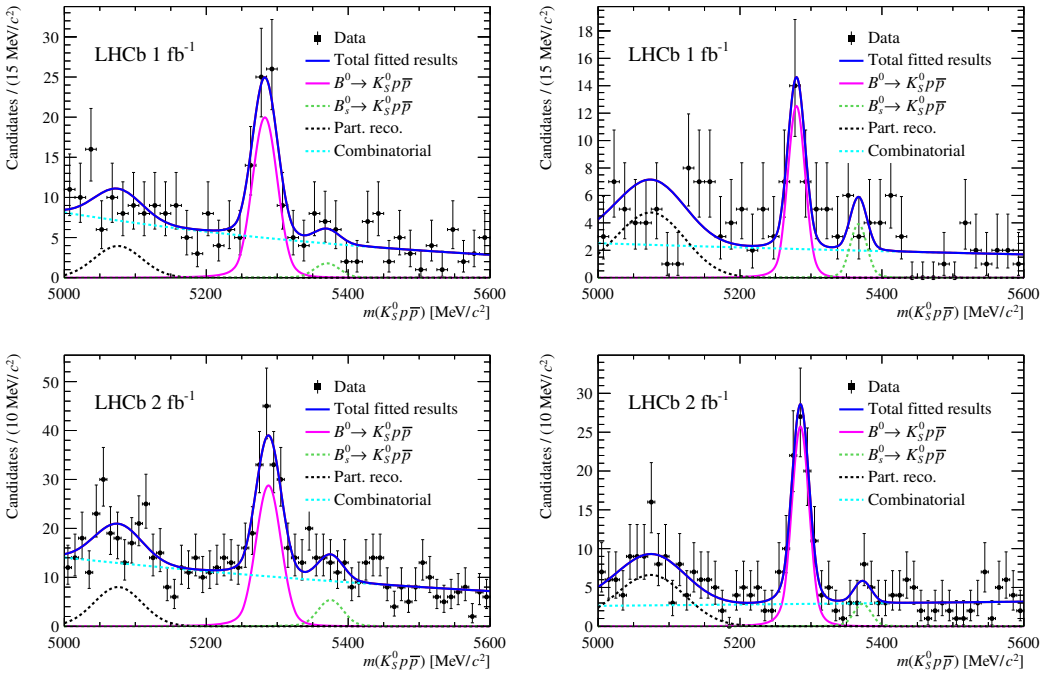

Figure 2. Invariant-mass distributions of $K^0_S p\overline{p}$ candidates passing the $B^0 \to K^0_S p\overline{p}$ selection. Data corresponding to (left) downstream and (right) long K^0_S reconstruction categories are shown for (top) the 2011 dataset and (bottom) the 2012 dataset. Fit results are also shown.

IPhU and Labex P2IO, and Région Auvergne-Rhône-Alpes (France); Alexander-von-Humboldt Foundation (Germany); ICSC (Italy); Severo Ochoa and María de Maeztu Units of Excellence, GVA, XuntaGal, GENCAT, InTalent-Inditex and Prog. Atracción Talento CM (Spain); SRC (Sweden); the Leverhulme Trust, the Royal Society and UKRI (United Kingdom).

A Fit results of all subsamples

The invariant-mass distributions for $B^0 \to K^0_S p\overline{p}$ candidates (optimised for the branching fraction measurement) are shown in figures 2 and 3 for Run 1 and Run 2, respectively, while figures 4 and 5 present the corresponding distributions for $B^0 \to K^0_S \pi^+\pi^-$ candidates. The $B^0_s \to K^0_S p\overline{p}$ candidates (optimised for search) distributions appear in figure 6. All analyses distinguish between downstream and long K^0_S reconstruction types, with the corresponding fit results and signal yields summarised in table 2.

JHEP07(2025)121

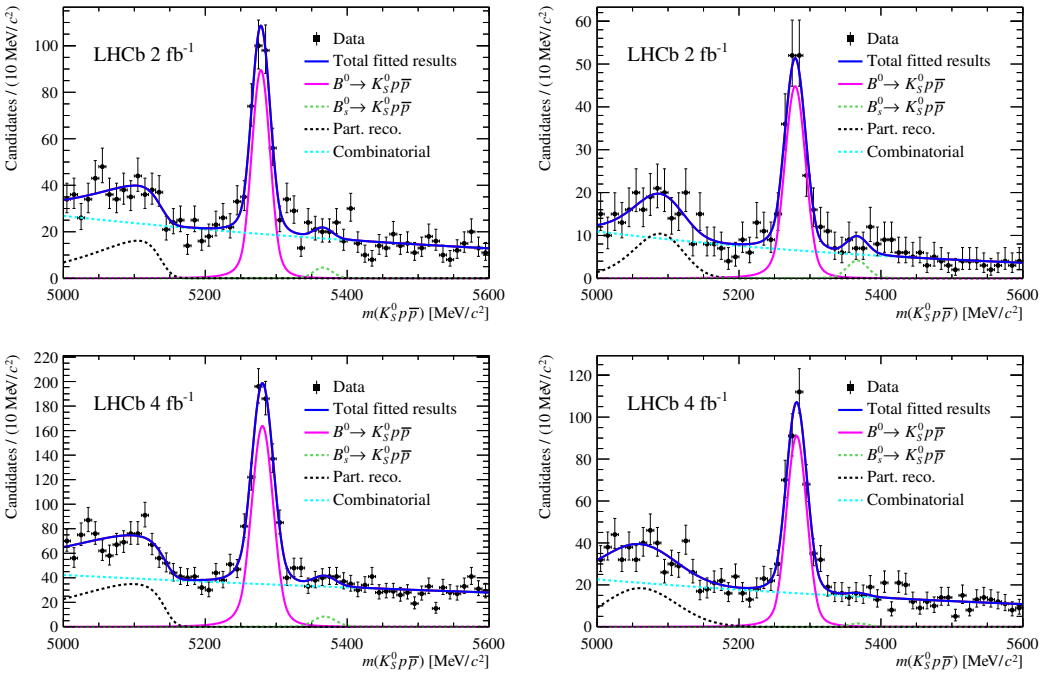

Figure 3. Invariant-mass distributions of $K^0_S p\overline{p}$ candidates passing the $B^0 \to K^0_S p\overline{p}$ selection. Data corresponding to (left) downstream and (right) long K^0_S reconstruction categories are shown for (top) the 2015–2016 dataset and (bottom) the 2017–2018 dataset. Fit results are also shown.

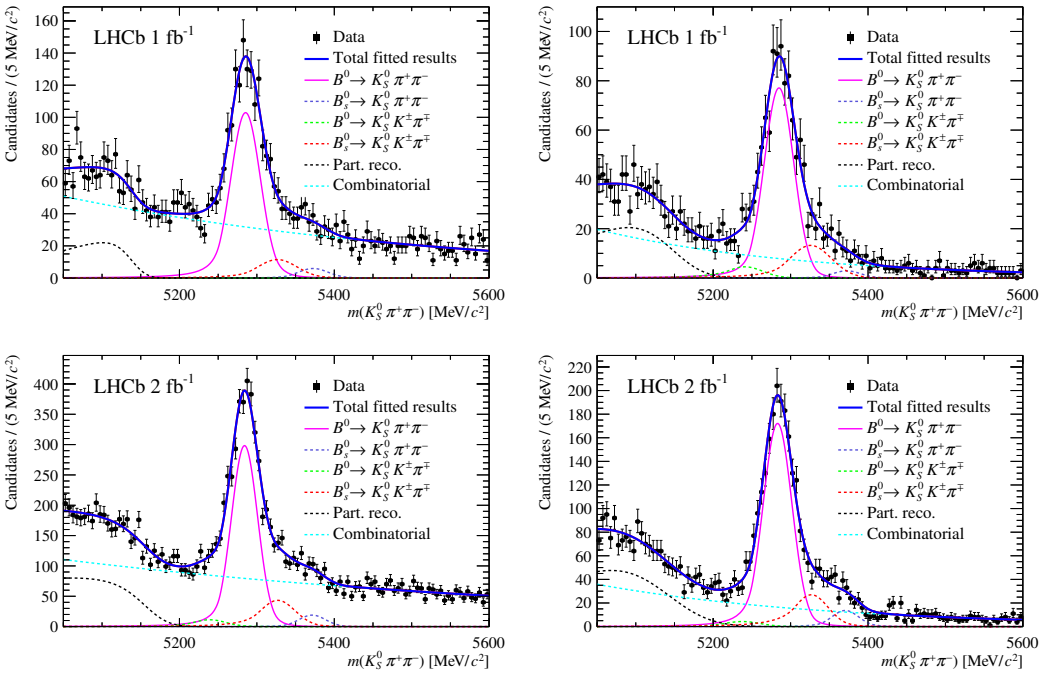

Figure 4. Invariant-mass distributions of $K^0_S\pi^+\pi^-$ candidates passing the $B^0 \to K^0_S\pi^+\pi^-$ selection. Data corresponding to (left) downstream and (right) long K^0_S reconstruction categories are shown for (top) the 2011 dataset and (bottom) the 2012 dataset. Fit results are also shown.

JHEP07(2025)121

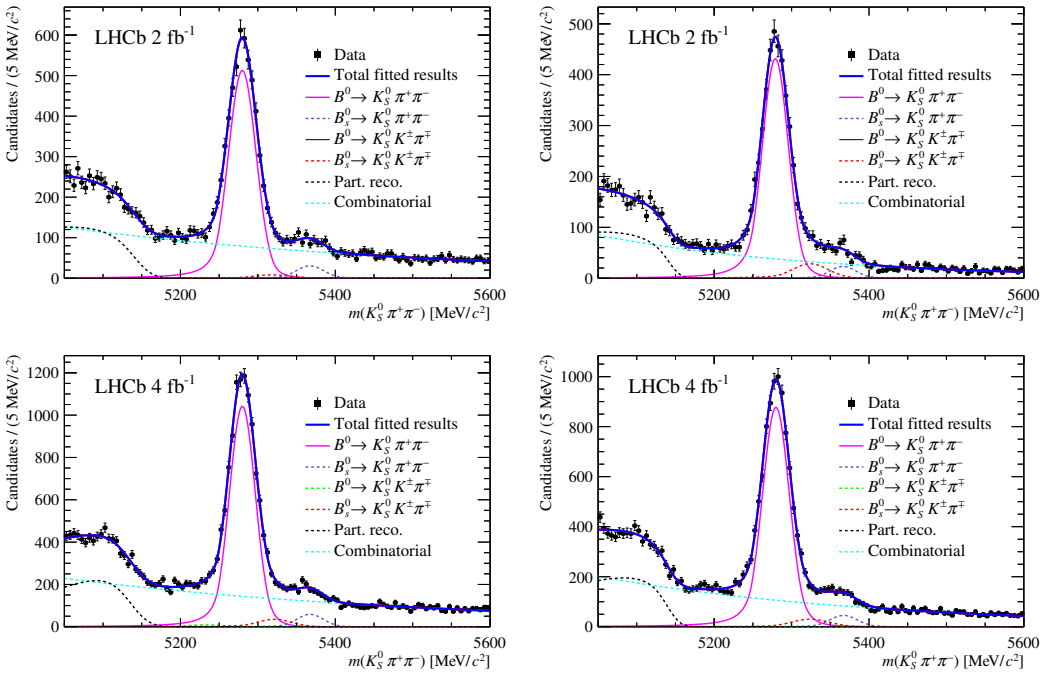

Figure 5. Invariant-mass distributions of $K^0_S\pi^+\pi^-$ candidates passing the $B^0 \to K^0_S\pi^+\pi^-$ selection. Data corresponding to (left) downstream and (right) long K^0_S reconstruction categories are shown for (top) the 2015–2016 dataset and (bottom) the 2017–2018 dataset. Fit results are also shown.

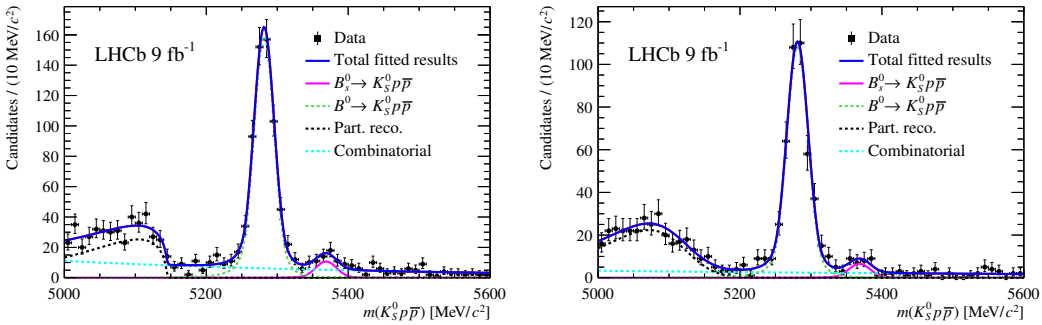

Figure 6. Invariant-mass distributions of $K^0_S p\overline{p}$ candidates passing the $B^0_s \to K^0_S p\overline{p}$ selection in the full dataset for (left) downstream and (right) long K^0_S reconstruction categories. Fit results are also shown.

JHEP07(2025)121

Modes	K^0_S	2011	2012	2015–2016	2017–2018
$B^0 \to K^0_S p\bar{p}$	Downstream	55 ± 9	135 ± 18	303 ± 24	670 ± 33
	Long	25 ± 7	83 ± 12	174 ± 18	346 ± 25
$B^0 \to K^0_S \pi^+\pi^-$	Downstream	1044 ± 65	2653 ± 96	4795 ± 108	9203 ± 143
	Long	772 ± 52	1678 ± 73	3892 ± 85	8109 ± 132
$B^0_s \to K^0_S p\bar{p}$	Downstream	41 ± 9			
	Long	26 ± 7			

Table 2. Signal yields for different decay channels and subsamples. The yields for the $B^0 \to K^0_S p\bar{p}$ decay are obtained from fits shown in figures 2 and 3, while the yields for the $B^0_s \to K^0_S p\bar{p}$ decay correspond to fits shown in figure 6. The quoted uncertainties are statistical only.

Data Availability Statement. Data associated with the plots in this publication asnwell as in supplementary materials are made available on the CERN document server at https://cds.cern.ch/record/2930997.

Code Availability Statement. This article has code included as electronic supplementary material.

References

[1] N. Cabibbo, *Unitary symmetry and leptonic decays*, *Phys. Rev. Lett.* **10** (1963) 531 [INSPIRE].

[2] J.L. Rosner, *Low mass baryon anti-baryon enhancements in B decays*, *Phys. Rev. D* **68** (2003) 014004 [hep-ph/0303079] [INSPIRE].

[3] BELLE collaboration, *Observation of $B^+ \to p\bar{p}\pi^+$, $B^0 \to p\bar{p}K^0$, and $B^+ \to p\bar{p}K^{*+}$*, *Phys. Rev. Lett.* **92** (2004) 131801 [hep-ex/0310018] [INSPIRE].

[4] C.Z. Yuan, X.H. Mo and P. Wang, *Baryon antibaryon nonets*, *Phys. Lett. B* **626** (2005) 95 [hep-ph/0506019] [INSPIRE].

[5] M. Suzuki, *Partial waves of baryon-antibaryon in three-body B meson decay*, *J. Phys. G* **34** (2007) 283 [hep-ph/0609133] [INSPIRE].

[6] V. Laporta, *Final stare interaction enhancement effect on the near threshold $p\bar{p}$ system in $B^\pm \to p\bar{p}\pi^\pm$ decay*, *Int. J. Mod. Phys. A* **22** (2007) 5401 [arXiv:0707.2751] [INSPIRE].

[7] BELLE collaboration, *Observation of $B^0 \to p\bar{p}K^{*0}$ with a large K^{*0} polarization*, *Phys. Rev. Lett.* **100** (2008) 251801 [arXiv:0802.0336] [INSPIRE].

[8] C.-K. Chua, W.-S. Hou and S.-Y. Tsai, *Charmless three-body baryonic B decays*, *Phys. Rev. D* **66** (2002) 054004 [hep-ph/0204185] [INSPIRE].

[9] C.Q. Geng and Y.K. Hsiao, *Angular distributions in three-body baryonic B decays*, *Phys. Rev. D* **74** (2006) 094023 [hep-ph/0606141] [INSPIRE].

[10] LHCb collaboration, *Amplitude analysis of $B^\pm \to \pi^\pm K^+ K^-$ decays*, *Phys. Rev. Lett.* **123** (2019) 231802 [arXiv:1905.09244] [INSPIRE].

JHEP07(2025)121

[11] Belle collaboration, *Dalitz analysis of three-body charmless $B^0 \to K^0\pi^+\pi^-$ decay*, *Phys. Rev. D* **75** (2007) 012006 [hep-ex/0610081] [INSPIRE].

[12] BaBar collaboration, *Time-dependent amplitude analysis of $B^0 \to K^0_S\pi^+\pi^-$*, *Phys. Rev. D* **80** (2009) 112001 [arXiv:0905.3615] [INSPIRE].

[13] Particle Data Group collaboration, *Review of particle physics*, *Phys. Rev. D* **110** (2024) 030001 [INSPIRE].

[14] BaBar collaboration, *Evidence for the $B^0 \to p\bar{p}K^{*0}$ and $B^+ \to \eta_c K^{*+}$ decays and study of the decay dynamics of B meson decays into $p\bar{p}h$ final states*, *Phys. Rev. D* **76** (2007) 092004 [arXiv:0707.1648] [INSPIRE].

[15] LHCb collaboration, *The LHCb detector at the LHC*, 2008 *JINST* **3** S08005 [INSPIRE].

[16] LHCb collaboration, *LHCb detector performance*, *Int. J. Mod. Phys. A* **30** (2015) 1530022 [arXiv:1412.6352] [INSPIRE].

[17] R. Aaij et al., *Performance of the LHCb vertex locator*, 2014 *JINST* **9** P09007 [arXiv:1405.7808] [INSPIRE].

[18] LHCb Outer Tracker Group collaboration, *Performance of the LHCb outer tracker*, 2014 *JINST* **9** P01002 [arXiv:1311.3893] [INSPIRE].

[19] LHCb RICH Group collaboration, *Performance of the LHCb RICH detector at the LHC*, *Eur. Phys. J. C* **73** (2013) 2431 [arXiv:1211.6759] [INSPIRE].

[20] A.A. Alves Jr. et al., *Performance of the LHCb muon system*, 2013 *JINST* **8** P02022 [arXiv:1211.1346] [INSPIRE].

[21] LHCb collaboration, *Handling of the generation of primary events in Gauss, the LHCb simulation framework*, *J. Phys. Conf. Ser.* **331** (2011) 032047 [INSPIRE].

[22] D.J. Lange, *The EvtGen particle decay simulation package*, *Nucl. Instrum. Meth. A* **462** (2001) 152 [INSPIRE].

[23] P. Golonka and Z. Was, *PHOTOS Monte Carlo: a precision tool for QED corrections in Z and W decays*, *Eur. Phys. J. C* **45** (2006) 97 [hep-ph/0506026] [INSPIRE].

[24] J. Allison et al., *GEANT4 developments and applications*, *IEEE Trans. Nucl. Sci.* **53** (2006) 270 [INSPIRE].

[25] GEANT4 collaboration, *GEANT4 — a simulation toolkit*, *Nucl. Instrum. Meth. A* **506** (2003) 250 [INSPIRE].

[26] LHCb collaboration, *The LHCb simulation application, Gauss: design, evolution and experience*, *J. Phys. Conf. Ser.* **331** (2011) 032023 [INSPIRE].

[27] R. Aaij et al., *The LHCb trigger and its performance in 2011*, 2013 *JINST* **8** P04022 [arXiv:1211.3055] [INSPIRE].

[28] V.V. Gligorov and M. Williams, *Efficient, reliable and fast high-level triggering using a bonsai boosted decision tree*, 2013 *JINST* **8** P02013 [arXiv:1210.6861] [INSPIRE].

[29] T. Likhomanenko et al., *LHCb topological trigger reoptimization*, *J. Phys. Conf. Ser.* **664** (2015) 082025 [arXiv:1510.00572] [INSPIRE].

[30] LHCb collaboration, *Search for CP violation using $\hat{T}$-odd correlations in $B^0 \to p\bar{p}K^+\pi^-$ decays*, *Phys. Rev. D* **108** (2023) 032007 [arXiv:2205.08973] [INSPIRE].

[31] L. Breiman, J. Friedman, R.A. Olshen and C.J. Stone, *Classification and regression trees*, Chapman and Hall/CRC (2017) [DOI:10.1201/9781315139470] [INSPIRE].

JHEP07(2025)121

[32] Y. Freund and R.E. Schapire, *A decision-theoretic generalization of on-line learning and an application to boosting*, *J. Comput. Syst. Sci.* **55** (1997) 119 [INSPIRE].

[33] H. Voss, A. Hocker, J. Stelzer and F. Tegenfeldt, *TMVA, the toolkit for multivariate data analysis with ROOT*, *PoS* **ACAT** (2007) 040 [INSPIRE].

[34] G. Punzi, *Sensitivity of searches for new signals and its optimization*, *eConf C* **030908** (2003) MODT002 [physics/0308063] [INSPIRE].

[35] T. Skwarnicki, *A study of the radiative CASCADE transitions between the Upsilon-Prime and Upsilon resonances*, Ph.D. thesis, INP, Cracow, Poland (1986) [INSPIRE].

[36] ARGUS collaboration, *Search for hadronic $b \to u$ decays*, *Phys. Lett. B* **241** (1990) 278 [INSPIRE].

[37] S.S. Wilks, *The large-sample distribution of the likelihood ratio for testing composite hypotheses*, *Annals Math. Statist.* **9** (1938) 60 [INSPIRE].

[38] LHCb collaboration, *Precise measurement of the f_s/f_d ratio of fragmentation fractions and of B^0_s decay branching fractions*, *Phys. Rev. D* **104** (2021) 032005 [arXiv:2103.06810] [INSPIRE].

[39] BELLE collaboration, *Time-dependent Dalitz plot measurement of CP parameters in $B^0 \to K^0_s\pi^+\pi^-$ decays*, *Phys. Rev. D* **79** (2009) 072004 [arXiv:0811.3665] [INSPIRE].

[40] LHCb collaboration, *Amplitude analysis of $B^0_s \to K^0_S K^\pm\pi^\mp$ decays*, *JHEP* **06** (2019) 114 [arXiv:1902.07955] [INSPIRE].

[41] M. Pivk and F.R. Le Diberder, *SPlot: a statistical tool to unfold data distributions*, *Nucl. Instrum. Meth. A* **555** (2005) 356 [physics/0402083] [INSPIRE].

[42] ATLAS collaboration, *Prospect for a search for direct stau production in events with at least two hadronic taus and missing transverse momentum at the High Luminosity LHC with the ATLAS detector*, ATL-PHYS-PUB-2016-021, CERN, Geneva, Switzerland (2016).

[43] M. Calvo Gomez et al., *A tool for γ/π^0 separation at high energies*, LHCb-PUB-2015-016, CERN, Geneva, Switzerland (2015).

[44] C. Abellán Beteta et al., *Calibration and performance of the LHCb calorimeters in run 1 and 2 at the LHC*, arXiv:2008.11556 [INSPIRE].

[45] LHCb collaboration, *Observation of the semileptonic decay $B^+ \to p\bar{p}\mu^+\nu_\mu$*, *JHEP* **03** (2020) 146 [arXiv:1911.08187] [INSPIRE].

[46] K. De Bruyn et al., *Branching ratio measurements of B_s decays*, *Phys. Rev. D* **86** (2012) 014027 [arXiv:1204.1735] [INSPIRE].

[47] CDF collaboration, *Observation of $B^0_s \to J/\psi K^{*0}(892)$ and $B^0_s \to J/\psi K^0_S$ decays*, *Phys. Rev. D* **83** (2011) 052012 [arXiv:1102.1961] [INSPIRE].

[48] R. Nisius, *On the combination of correlated estimates of a physics observable*, *Eur. Phys. J. C* **74** (2014) 3004 [arXiv:1402.4016] [INSPIRE].

JHEP07(2025)121

The LHCb collaboration

R. Aaij[38], A.S.W. Abdelmotteleb[57], C. Abellan Beteta[51], F. Abudinén[57], T. Ackernley[61], A. A. Adefisoye[69], B. Adeva[47], M. Adinolfi[55], P. Adlarson[84], C. Agapopoulou[14], C.A. Aidala[86], Z. Ajaltouni[11], S. Akar[11], K. Akiba[38], P. Albicocco[28], J. Albrecht[19,e], F. Alessio[49], Z. Aliouche[63], P. Alvarez Cartelle[56], R. Amalric[16], S. Amato[3], J.L. Amey[55], Y. Amhis[14], L. An[6], L. Anderlini[27], M. Andersson[51], A. Andreianov[44], P. Andreola[51], M. Andreotti[26], D. Andreou[69], A. Anelli[31,o,49], D. Ao[7], F. Archilli[37,u], M. Argenton[26], S. Arguedas Cuendis[9,49], A. Artamonov[44], M. Artuso[69], E. Aslanides[13], R. Ataíde Da Silva[50], M. Atzeni[65], B. Audurier[12], D. Bacher[64], I. Bachiller Perea[50], S. Bachmann[22], M. Bachmayer[50], J.J. Back[57], P. Baladron Rodriguez[47], V. Balagura[15], A. Balboni[26], W. Baldini[26], L. Balzani[19], H. Bao[7], J. Baptista de Souza Leite[61], C. Barbero Pretel[47,12], M. Barbetti[27], I. R. Barbosa[70], R.J. Barlow[63], M. Barnyakov[25], S. Barsuk[14], W. Barter[59], J. Bartz[69], S. Bashir[40], B. Batsukh[5], P. B. Battista[14], A. Bay[50], A. Beck[65], M. Becker[19], F. Bedeschi[35], I.B. Bediaga[2], N. A. Behling[19], S. Belin[47], K. Belous[44], I. Belov[29], I. Belyaev[36], G. Benane[13], G. Bencivenni[28], E. Ben-Haim[16], A. Berezhnoy[44], R. Bernet[51], S. Bernet Andres[46], A. Bertolin[33], C. Betancourt[51], F. Betti[59], J. Bex[56], Ia. Bezshyiko[51], O. Bezshyyko[85], J. Bhom[41], M.S. Bieker[18], N.V. Biesuz[26], P. Billoir[16], A. Biolchini[38], M. Birch[62], F.C.R. Bishop[10], A. Bitadze[63], A. Bizzeti[], T. Blake[57], F. Blanc[50], J.E. Blank[19], S. Blusk[69], V. Bocharnikov[44], J.A. Boelhauve[19], O. Boente Garcia[15], T. Boettcher[68], A. Bohare[59], A. Boldyrev[44], C.S. Bolognani[81], R. Bolzonella[26], R. B. Bonacci[1], N. Bondar[44,49], A. Bordelius[49], F. Borgato[33,49], S. Borghi[63], M. Borsato[31,o], J.T. Borsuk[82], E. Bottalico[61], S.A. Bouchiba[50], M. Bovill[64], T.J.V. Bowcock[61], A. Boyer[49], C. Bozzi[26], J. D. Brandenburg[87], A. Brea Rodriguez[50], N. Breer[19], J. Brodzicka[41], A. Brossa Gonzalo[47,†], J. Brown[61], D. Brundu[32], E. Buchanan[59], L. Buonincontri[33,p], M. Burgos Marcos[81], A.T. Burke[63], C. Burr[49], J.S. Butter[56], J. Buytaert[49], W. Byczynski[49], S. Cadeddu[32], H. Cai[74], A. Caillet[16], R. Calabrese[26,k], S. Calderon Ramirez[9], L. Calefice[45], S. Cali[28], M. Calvi[31,o], M. Calvo Gomez[46], P. Camargo Magalhaes[2,z], J. I. Cambon Bouzas[47], P. Campana[28], D.H. Campora Perez[81], A.F. Campoverde Quezada[7], S. Capelli[31], L. Capriotti[26], R. Caravaca-Mora[9], A. Carbone[25,i], L. Carcedo Salgado[47], R. Cardinale[29,m], A. Cardini[32], P. Carniti[31,o], L. Carus[22], A. Casais Vidal[65], R. Caspary[22], G. Casse[61], M. Cattaneo[49], G. Cavallero[26,49], V. Cavallini[26,k], S. Celani[22], S. Cesare[30,n], A.J. Chadwick[61], I. Chahrour[86], H. Chang[4,b], M. Charles[16], Ph. Charpentier[49], E. Chatzianagnostou[38], M. Chefdeville[10], C. Chen[56], S. Chen[5], Z. Chen[7], A. Chernov[41], S. Chernyshenko[53], X. Chiotopoulos[81], V. Chobanova[83], M. Chrzaszcz[41], A. Chubykin[44], V. Chulikov[28,36], P. Ciambrone[28], X. Cid Vidal[47], G. Ciezarek[49], P. Cifra[49], P.E.L. Clarke[59], M. Clemencic[49], H.V. Cliff[56], J. Closier[49], C. Cocha Toapaxi[22], V. Coco[49], J. Cogan[13], E. Cogneras[11], L. Cojocariu[43], S. Collaviti[50], P. Collins[49], T. Colombo[49], M. Colonna[19], A. Comerma-Montells[45], L. Congedo[24], A. Contu[32], N. Cooke[60], C. Coronel[66], I. Corredoira[12], A. Correia[16], G. Corti[49], J. Cottee Meldrum[55], B. Couturier[49], D.C. Craik[51], M. Cruz Torres[2,f], E. Curras Rivera[50], R. Currie[59], C.L. Da Silva[68], S. Dadabaev[44], L. Dai[71], X. Dai[4], E. Dall'Occo[49], J. Dalseno[83], C. D'Ambrosio[62], J. Daniel[11], P. d'Argent[24], G. Darze[3], A.

JHEP07(2025)121

Davidson[57], J.E. Davies[63], O. De Aguiar Francisco[63], C. De Angelis[32,j], F. De Benedetti[49], J. de Boer[38], K. De Bruyn[80], S. De Capua[63], M. De Cian[22], U. De Freitas Carneiro Da Graca[2,a], E. De Lucia[28], J.M. De Miranda[2], L. De Paula[3], M. De Serio[24,g], P. De Simone[28], F. De Vellis[19], J.A. de Vries[81], F. Debernardis[24], D. Decamp[10], S. Dekkers[1], L. Del Buono[16], B. Delaney[65], H.-P. Dembinski[19], J. Deng[8], V. Denysenko[51], O. Deschamps[11], F. Dettori[32,j], B. Dey[78], P. Di Nezza[28], I. Diachkov[44], S. Didenko[44], S. Ding[69], L. Dittmann[22], V. Dobishuk[53], A. D. Docheva[60], C. Dong[4,b], A.M. Donohoe[23], F. Dordei[32], A.C. dos Reis[2], A. D. Dowling[69], W. Duan[72], P. Duda[82], M.W. Dudek[41], L. Dufour[49], V. Duk[34], P. Durante[49], M. M. Duras[82], J.M. Durham[68], O. D. Durmus[78], A. Dziurda[41], A. Dzyuba[44], S. Easo[58], E. Eckstein[18], U. Egede[1], A. Egorychev[44], V. Egorychev[44], S. Eisenhardt[59], E. Ejopu[63], L. Eklund[84], M. Elashri[66], J. Ellbracht[19], S. Ely[62], A. Ene[43], J. Eschle[69], S. Esen[22], T. Evans[38], F. Fabiano[32], S. Faghih[66], L.N. Falcao[2], B. Fang[7], L. Fantini[34,q,49], M. Faria[50], K. Farmer[59], D. Fazzini[31,o], L. Felkowski[82], M. Feng[5,7], M. Feo[2], A. Fernandez Casani[48], M. Fernandez Gomez[47], A.D. Fernez[67], F. Ferrari[25,i], F. Ferreira Rodrigues[3], M. Ferrillo[51], M. Ferro-Luzzi[49], S. Filippov[44], R.A. Fini[24], M. Fiorini[26,k], M. Firlej[40], K.L. Fischer[64], D.S. Fitzgerald[86], C. Fitzpatrick[63], T. Fiutowski[40], F. Fleuret[15], M. Fontana[25], L. F. Foreman[63], R. Forty[49], D. Foulds-Holt[56], V. Franco Lima[3], M. Franco Sevilla[67], M. Frank[49], E. Franzoso[26,k], G. Frau[63], C. Frei[49], D.A. Friday[63], J. Fu[7], Q. Führing[19,e,56], Y. Fujii[1], T. Fulghesu[13], E. Gabriel[38], G. Galati[24], M.D. Galati[38], A. Gallas Torreira[47], D. Galli[25,i], S. Gambetta[59], M. Gandelman[3], P. Gandini[30], B. Ganie[63], H. Gao[7], R. Gao[64], T.Q. Gao[56], Y. Gao[8], Y. Gao[6], Y. Gao[8], L.M. Garcia Martin[50], P. Garcia Moreno[45], J. García Pardiñas[65], P. Gardner[67], K. G. Garg[8], L. Garrido[45], C. Gaspar[49], A. Gavrikov[33], L.L. Gerken[19], E. Gersabeck[20], M. Gersabeck[20], T. Gershon[57], S. Ghizzo[29,m], Z. Ghorbanimoghaddam[55], L. Giambastiani[33,p], F. I. Giasemis[16,d], V. Gibson[56], H.K. Giemza[42], A.L. Gilman[64], M. Giovannetti[28], A. Gioventù[45], L. Girardey[63,58], C. Giugliano[26,k], M.A. Giza[41], F.C. Glaser[14,22], V.V. Gligorov[16], C. Göbel[70], L. Golinka-Bezshyyko[85], E. Golobardes[46], D. Golubkov[44], A. Golutvin[62,49], S. Gomez Fernandez[45], W. Gomulka[40], F. Goncalves Abrantes[64], M. Goncerz[41], G. Gong[4,b], J. A. Gooding[19], I.V. Gorelov[44], C. Gotti[31], E. Govorkova[65], J.P. Grabowski[18], L.A. Granado Cardoso[49], E. Graugés[45], E. Graverini[50,s], L. Grazette[57], G. Graziani[], A. T. Grecu[43], L.M. Greeven[38], N.A. Grieser[66], L. Grillo[60], S. Gromov[44], C. Gu[15], M. Guarise[26], L. Guerry[11], V. Guliaeva[44], P. A. Günther[22], A.-K. Guseinov[50], E. Gushchin[44], Y. Guz[6,49], T. Gys[49], K. Habermann[18], T. Hadavizadeh[1], C. Hadjivasiliou[67], G. Haefeli[50], C. Haen[49], G. Hallett[57], P.M. Hamilton[67], J. Hammerich[61], Q. Han[33], X. Han[22,49], S. Hansmann-Menzemer[22], L. Hao[7], N. Harnew[64], T. H. Harris[1], M. Hartmann[14], S. Hashmi[40], J. He[7,c], F. Hemmer[49], C. Henderson[66], R.D.L. Henderson[1,57], A.M. Hennequin[49], K. Hennessy[61], L. Henry[50], J. Herd[62], P. Herrero Gascon[22], J. Heuel[17], A. Hicheur[3], G. Hijano Mendizabal[51], J. Horswill[63], R. Hou[8], Y. Hou[11], N. Howarth[61], J. Hu[72], W. Hu[7], X. Hu[4,b], W. Hulsbergen[38], R.J. Hunter[57], M. Hushchyn[44], D. Hutchcroft[61], M. Idzik[40], D. Ilin[44], P. Ilten[66], A. Inglessi[44], A. Iniukhin[44], A. Ishteev[44], K. Ivshin[44], H. Jage[17], S.J. Jaimes Elles[76,49,48],

JHEP07(2025)121

S. Jakobsen[49], E. Jans[38], B.K. Jashal[48], A. Jawahery[67], V. Jevtic[19], E. Jiang[67], X. Jiang[5,7], Y. Jiang[7], Y. J. Jiang[6], M. John[64], A. John Rubesh Rajan[23], D. Johnson[54], C.R. Jones[56], T.P. Jones[57], S. Joshi[42], B. Jost[49], J. Juan Castella[56], N. Jurik[49], I. Juszczak[41], D. Kaminaris[50], S. Kandybei[52], M. Kane[59], Y. Kang[4,b], C. Kar[11], M. Karacson[49], D. Karpenkov[44], A. Kauniskangas[50], J.W. Kautz[66], M.K. Kazanecki[41], F. Keizer[49], M. Kenzie[56], T. Ketel[38], B. Khanji[69], A. Kharisova[44], S. Kholodenko[35,49], G. Khreich[14], T. Kirn[17], V.S. Kirsebom[31,o], O. Kitouni[65], S. Klaver[39], N. Kleijne[35,r], K. Klimaszewski[42], M.R. Kmiec[42], S. Koliiev[53], L. Kolk[19], A. Konoplyannikov[6], P. Kopciewicz[49], P. Koppenburg[38], A. Korchin[52], M. Korolev[44], I. Kostiuk[38], O. Kot[53], S. Kotriakhova, A. Kozachuk[44], P. Kravchenko[44], L. Kravchuk[44], M. Kreps[57], P. Krokovny[44], W. Krupa[69], W. Krzemien[42], O. Kshyvanskyi[53], S. Kubis[82], M. Kucharczyk[41], V. Kudryavtsev[44], E. Kulikova[44], A. Kupsc[84], V. Kushnir[52], B. Kutsenko[13], I. Kyryllin[52], D. Lacarrere[49], P. Laguarta Gonzalez[45], A. Lai[32], A. Lampis[32], D. Lancierini[62], C. Landesa Gomez[47], J.J. Lane[1], G. Lanfranchi[28], C. Langenbruch[22], J. Langer[19], O. Lantwin[44], T. Latham[57], F. Lazzari[35,s,49], C. Lazzeroni[54], R. Le Gac[13], H. Lee[61], R. Lefèvre[11], A. Leflat[44], S. Legotin[44], M. Lehuraux[57], E. Lemos Cid[49], O. Leroy[13], T. Lesiak[41], E. D. Lesser[49], B. Leverington[22], A. Li[4,b], C. Li[4], C. Li[13], H. Li[72], J. Li[8], K. Li[75], L. Li[63], M. Li[8], P. Li[7], P.-R. Li[73], Q. Li[5,7], S. Li[8], T. Li[71], T. Li[72], Y. Li[8], Y. Li[5], Z. Lian[4,b], X. Liang[69], S. Libralon[48], C. Lin[7], T. Lin[58], R. Lindner[49], H. Linton[62], V. Lisovskyi[50], R. Litvinov[32,49], D. Liu[8], F. L. Liu[1], G. Liu[72], K. Liu[73], S. Liu[5,7], W. Liu[8], Y. Liu[59], Y. Liu[73], Y. L. Liu[62], G. Loachamin Ordonez[70], A. Lobo Salvia[45], A. Loi[32], T. Long[56], J.H. Lopes[3], A. Lopez Huertas[45], S. López Soliño[47], Q. Lu[15], C. Lucarelli[27,l], D. Lucchesi[33,p], M. Lucio Martinez[48], Y. Luo[6], A. Lupato[33,h], E. Luppi[26,k], K. Lynch[23], X.-R. Lyu[7], G. M. Ma[4,b], S. Maccolini[19], F. Machefert[14], F. Maciuc[43], B. Mack[69], I. Mackay[64], L. M. Mackey[69], L.R. Madhan Mohan[56], M. J. Madurai[54], D. Magdalinski[38], D. Maisuzenko[44], J.J. Malczewski[41], S. Malde[64], L. Malentacca[49], A. Malinin[44], T. Maltsev[44], G. Manca[32,j], G. Mancinelli[13], C. Mancuso[14], R. Manera Escalero[45], F. M. Manganella[37], D. Manuzzi[25], D. Marangotto[30], J.F. Marchand[10], R. Marchevski[50], U. Marconi[25], E. Mariani[16], S. Mariani[49], C. Marin Benito[45], J. Marks[22], A.M. Marshall[55], L. Martel[64], G. Martelli[34,q], G. Martellotti[36], L. Martinazzoli[49], M. Martinelli[31,o], D. Martinez Gomez[80], D. Martinez Santos[83], F. Martinez Vidal[48], A. Martorell i Granollers[46], A. Massafferri[2], R. Matev[49], A. Mathad[49], V. Matiunin[44], C. Matteuzzi[69], K.R. Mattioli[15], A. Mauri[62], E. Maurice[15], J. Mauricio[45], P. Mayencourt[50], J. Mazorra de Cos[48], M. Mazurek[42], M. McCann[62], T.H. McGrath[63], N.T. McHugh[60], A. McNab[63], R. McNulty[23], B. Meadows[66], G. Meier[19], D. Melnychuk[42], F. M. Meng[4,b], M. Merk[38,81], A. Merli[50], L. Meyer Garcia[67], D. Miao[5,7], H. Miao[7], M. Mikhasenko[77], D.A. Milanes[76,x], A. Minotti[31,o], E. Minucci[28], T. Miralles[11], B. Mitreska[19], D.S. Mitzel[19], A. Modak[58], L. Moeser[19], R.A. Mohammed[64], R.D. Moise[17], E. F. Molina Cardenas[86], T. Mombächer[49], M. Monk[57,1], S. Monteil[11], A. Morcillo Gomez[47], G. Morello[28], M.J. Morello[35,r], M.P. Morgenthaler[22], J. Moron[40], W. Morren[38], A.B. Morris[49], A.G. Morris[13], R. Mountain[69], H. Mu[4,b], Z. M. Mu[6],

JHEP07(2025)121

E. Muhammad[57], F. Muheim[59], M. Mulder[80], K. Müller[51], F. Muñoz-Rojas[9], R. Murta[62], V. Mytrochenko[52], P. Naik[61], T. Nakada[50], R. Nandakumar[58], T. Nanut[49], I. Nasteva[3], M. Needham[59], E. Nekrasova[44], N. Neri[30,n], S. Neubert[18], N. Neufeld[49], P. Neustroev[44], J. Nicolini[49], D. Nicotra[81], E.M. Niel[49], N. Nikitin[44], Q. Niu[73], P. Nogarolli[3], P. Nogga[18], C. Normand[55], J. Novoa Fernandez[47], G. Nowak[66], C. Nunez[86], H. N. Nur[60], A. Oblakowska-Mucha[40], V. Obraztsov[44], T. Oeser[17], S. Okamura[26,k], A. Okhotnikov[44], O. Okhrimenko[53], R. Oldeman[32,j], F. Oliva[59], M. Olocco[19], C.J.G. Onderwater[81], R.H. O'Neil[49], D. Osthues[19], J.M. Otalora Goicochea[3], P. Owen[51], A. Oyanguren[48], O. Ozcelik[59], F. Paciolla[35,v], A. Padee[42], K.O. Padeken[18], B. Pagare[57], T. Pajero[49], A. Palano[24], M. Palutan[28], X. Pan[4,b], S. Panebianco[12], G. Panshin[5], L. Paolucci[57], A. Papanestis[58,49], M. Pappagallo[24,g], L.L. Pappalardo[26], C. Pappenheimer[66], C. Parkes[63], D. Parmar[77], B. Passalacqua[26,k], G. Passaleva[27], D. Passaro[35,r,49], A. Pastore[24], M. Patel[62], J. Patoc[64], C. Patrignani[25,i], A. Paul[69], C.J. Pawley[81], A. Pellegrino[38], J. Peng[5,7], M. Pepe Altarelli[28], S. Perazzini[25], D. Pereima[44], H. Pereira Da Costa[68], A. Pereiro Castro[47], P. Perret[11], A. Perrevoort[80], A. Perro[49,13], M.J. Peters[66], K. Petridis[55], A. Petrolini[29,m], J. P. Pfaller[66], H. Pham[69], L. Pica[35], M. Piccini[34], L. Piccolo[32], B. Pietrzyk[10], G. Pietrzyk[14], R. N. Pilato[61], D. Pinci[36], F. Pisani[49], M. Pizzichemi[31,o,49], V. M. Placinta[43], M. Plo Casasus[47], T. Poeschl[49], F. Polci[16], M. Poli Lener[28], A. Poluektov[13], N. Polukhina[44], I. Polyakov[63], E. Polycarpo[3], S. Ponce[49], D. Popov[7,49], S. Poslavskii[44], K. Prasanth[59], C. Prouve[83], D. Provenzano[32,j], V. Pugatch[53], G. Punzi[35,s], S. Qasim[51], Q. Q. Qian[6], W. Qian[7], N. Qin[4,b], S. Qu[4,b], R. Quagliani[49], R.I. Rabadan Trejo[57], J.H. Rademacker[55], M. Rama[35], M. Ramírez García[86], V. Ramos De Oliveira[70], M. Ramos Pernas[57], M.S. Rangel[3], F. Ratnikov[44], G. Raven[39], M. Rebollo De Miguel[48], F. Redi[30,h], J. Reich[55], F. Reiss[20], Z. Ren[7], P.K. Resmi[64], M. Ribalda Galvez[45], R. Ribatti[50], G. Ricart[15,12], D. Riccardi[35,r], S. Ricciardi[58], K. Richardson[65], M. Richardson-Slipper[59], K. Rinnert[61], P. Robbe[14,49], G. Robertson[60], E. Rodrigues[61], A. Rodriguez Alvarez[45], E. Rodriguez Fernandez[47], J.A. Rodriguez Lopez[76], E. Rodriguez Rodriguez[49], J. Roensch[19], A. Rogachev[44], A. Rogovskiy[58], D.L. Rolf[19], P. Roloff[49], V. Romanovskiy[66], A. Romero Vidal[47], G. Romolini[26], F. Ronchetti[50], T. Rong[6], M. Rotondo[28], S. R. Roy[22], M.S. Rudolph[69], M. Ruiz Diaz[22], R.A. Ruiz Fernandez[47], J. Ruiz Vidal[81], J. J. Saavedra-Arias[9], J.J. Saborido Silva[47], R. Sadek[15], N. Sagidova[44], D. Sahoo[78], N. Sahoo[54], B. Saitta[32,j], M. Salomoni[31,49,o], I. Sanderswood[48], R. Santacesaria[36], C. Santamarina Rios[47], M. Santimaria[28], L. Santoro[2], E. Santovetti[37], A. Saputi[26,49], D. Saranin[44], A. Sarnatskiy[80], G. Sarpis[59], M. Sarpis[79], C. Satriano[36,t], A. Satta[37], M. Saur[73], D. Savrina[44], H. Sazak[17], F. Sborzacchi[49,28], A. Scarabotto[19], S. Schael[17], S. Scherl[61], M. Schiller[60], H. Schindler[49], M. Schmelling[21], B. Schmidt[49], S. Schmitt[17], H. Schmitz[18], O. Schneider[50], A. Schopper[62], N. Schulte[19], S. Schulte[50], M.H. Schune[14], G. Schwering[17], B. Sciascia[28], A. Sciuccati[49], I. Segal[77], S. Sellam[47], A. Semennikov[44], T. Senger[51], M. Senghi Soares[39], A. Sergi[29,m], N. Serra[51], L. Sestini[27], A. Seuthe[19], B. Sevilla Sanjuan[46], Y. Shang[6], D.M. Shangase[86], M. Shapkin[44], R. S. Sharma[69], I. Shchemerov[44], L. Shchutska[50], T. Shears[61], L. Shekhtman[44], Z. Shen[38], S. Sheng[5,7], V. Shevchenko[44], B. Shi[7], Q. Shi[7], Y. Shimizu[14], E. Shmanin[25], R. Shorkin[44],

JHEP07(2025)121

J.D. Shupperd[69], R. Silva Coutinho[69], G. Simi[33,p], S. Simone[24,g], M. Singha[78], N. Skidmore[57], T. Skwarnicki[69], M.W. Slater[54], E. Smith[65], K. Smith[68], M. Smith[62], L. Soares Lavra[59], M.D. Sokoloff[66], F.J.P. Soler[60], A. Solomin[55], A. Solovev[44], I. Solovyev[44], N. S. Sommerfeld[18], R. Song[1], Y. Song[50], Y. Song[4,b], Y. S. Song[6], F.L. Souza De Almeida[69], B. Souza De Paula[3], E. Spadaro Norella[29,m], E. Spedicato[25], J.G. Speer[19], E. Spiridenkov[44], P. Spradlin[60], V. Sriskaran[49], F. Stagni[49], M. Stahl[77], S. Stahl[49], S. Stanislaus[64], M. Stefaniak[87], E.N. Stein[49], O. Steinkamp[51], O. Stenyakin[44], H. Stevens[19], D. Strekalina[44], Y. Su[7], F. Suljik[64], J. Sun[32], L. Sun[74], D. Sundfeld[2], W. Sutcliffe[51], K. Swientek[40], F. Swystun[56], A. Szabelski[42], T. Szumlak[40], Y. Tan[4,b], Y. Tang[74], Y. T. Tang[7], M.D. Tat[22], A. Terentev[44], F. Terzuoli[35,v,49], F. Teubert[49], U. Thoma[18], E. Thomas[49], D.J.D. Thompson[54], H. Tilquin[62], V. Tisserand[11], S. T'Jampens[10], M. Tobin[5], L. Tomassetti[26,k], G. Tonani[30,n], X. Tong[6], T. Tork[30], D. Torres Machado[2], L. Toscano[19], D.Y. Tou[4,b], C. Trippl[46], G. Tuci[22], N. Tuning[38], L.H. Uecker[22], A. Ukleja[40], D.J. Unverzagt[22], A. Upadhyay[78], B. Urbach[59], A. Usachov[39], A. Ustyuzhanin[44], U. Uwer[22], V. Vagnoni[25], V. Valcarce Cadenas[47], G. Valenti[25], N. Valls Canudas[49], J. van Eldik[49], H. Van Hecke[68], E. van Herwijnen[62], C.B. Van Hulse[47,y], R. Van Laak[50], M. van Veghel[38], G. Vasquez[51], R. Vazquez Gomez[45], P. Vazquez Regueiro[47], C. Vázquez Sierra[83], S. Vecchi[26], J.J. Velthuis[55], M. Veltri[27,w], A. Venkateswaran[50], M. Verdoglia[32], M. Vesterinen[57], D. Vico Benet[64], P. Vidrier Villalba[45], M. Vieites Diaz[47], X. Vilasis-Cardona[46], E. Vilella Figueras[61], A. Villa[25], P. Vincent[16], B. Vivacqua[3], F.C. Volle[54], D. vom Bruch[13], N. Voropaev[44], K. Vos[81], C. Vrahas[59], J. Wagner[19], J. Walsh[35], E.J. Walton[1,57], G. Wan[6], A. Wang[7], C. Wang[22], G. Wang[8], H. Wang[73], J. Wang[6], J. Wang[5], J. Wang[4,b], J. Wang[74], M. Wang[49], N. W. Wang[7], R. Wang[55], X. Wang[8], X. Wang[72], X. W. Wang[62], Y. Wang[75], Y. Wang[6], Y. W. Wang[73], Z. Wang[14], Z. Wang[4,b], Z. Wang[30], J.A. Ward[57,1], M. Waterlaat[49], N.K. Watson[54], D. Websdale[62], Y. Wei[6], J. Wendel[83], B.D.C. Westhenry[55], C. White[56], M. Whitehead[60], E. Whiter[54], A.R. Wiederhold[63], D. Wiedner[19], G. Wilkinson[64,49], M.K. Wilkinson[66], M. Williams[65], M. J. Williams[49], M.R.J. Williams[59], R. Williams[56], Z. Williams[55], F.F. Wilson[58], M. Winn[12], W. Wislicki[42], M. Witek[41], L. Witola[19], G. Wormser[14], S.A. Wotton[56], H. Wu[69], J. Wu[8], X. Wu[74], Y. Wu[6,56], Z. Wu[7], K. Wyllie[49], S. Xian[72], Z. Xiang[5], Y. Xie[8], T. X. Xing[30], A. Xu[35], L. Xu[4,b], L. Xu[4,b], M. Xu[57], Z. Xu[49], Z. Xu[7], Z. Xu[5], K. Yang[62], X. Yang[6], Y. Yang[29,m], Z. Yang[6], V. Yeroshenko[14], H. Yeung[63], H. Yin[8], X. Yin[7], C. Y. Yu[6], J. Yu[71], X. Yuan[5], Y Yuan[5,7], E. Zaffaroni[50], M. Zavertyaev[21], M. Zdybal[41], F. Zenesini[25], C. Zeng[5,7], M. Zeng[4,b], C. Zhang[6], D. Zhang[8], J. Zhang[7], L. Zhang[4,b], R. Zhang[8], S. Zhang[71], S. Zhang[64], Y. Zhang[6], Y. Z. Zhang[4,b], Z. Zhang[4,b], Y. Zhao[22], A. Zhelezov[22], S. Z. Zheng[6], X. Z. Zheng[4,b], Y. Zheng[7], T. Zhou[6], X. Zhou[8], Y. Zhou[7], V. Zhovkovska[57], L. Z. Zhu[7], X. Zhu[4,b], X. Zhu[8], Y. Zhu[17], V. Zhukov[17], J. Zhuo[48], Q. Zou[5,7], D. Zuliani[33,p], G. Zunica[50]

[1] *School of Physics and Astronomy, Monash University, Melbourne, Australia*
[2] *Centro Brasileiro de Pesquisas Físicas (CBPF), Rio de Janeiro, Brazil*
[3] *Universidade Federal do Rio de Janeiro (UFRJ), Rio de Janeiro, Brazil*
[4] *Department of Engineering Physics, Tsinghua University, Beijing, China*
[5] *Institute Of High Energy Physics (IHEP), Beijing, China*

JHEP07(2025)121

[6] School of Physics State Key Laboratory of Nuclear Physics and Technology, Peking University, Beijing, China
[7] University of Chinese Academy of Sciences, Beijing, China
[8] Institute of Particle Physics, Central China Normal University, Wuhan, Hubei, China
[9] Consejo Nacional de Rectores (CONARE), San Jose, Costa Rica
[10] Université Savoie Mont Blanc, CNRS, IN2P3-LAPP, Annecy, France
[11] Université Clermont Auvergne, CNRS/IN2P3, LPC, Clermont-Ferrand, France
[12] Université Paris-Saclay, Centre d'Etudes de Saclay (CEA), IRFU, Saclay, France, Gif-Sur-Yvette, France
[13] Aix Marseille Univ, CNRS/IN2P3, CPPM, Marseille, France
[14] Université Paris-Saclay, CNRS/IN2P3, IJCLab, Orsay, France
[15] Laboratoire Leprince-Ringuet, CNRS/IN2P3, Ecole Polytechnique, Institut Polytechnique de Paris, Palaiseau, France
[16] LPNHE, Sorbonne Université, Paris Diderot Sorbonne Paris Cité, CNRS/IN2P3, Paris, France
[17] I. Physikalisches Institut, RWTH Aachen University, Aachen, Germany
[18] Universität Bonn — Helmholtz-Institut für Strahlen und Kernphysik, Bonn, Germany
[19] Fakultät Physik, Technische Universität Dortmund, Dortmund, Germany
[20] Physikalisches Institut, Albert-Ludwigs-Universität Freiburg, Freiburg, Germany
[21] Max-Planck-Institut für Kernphysik (MPIK), Heidelberg, Germany
[22] Physikalisches Institut, Ruprecht-Karls-Universität Heidelberg, Heidelberg, Germany
[23] School of Physics, University College Dublin, Dublin, Ireland
[24] INFN Sezione di Bari, Bari, Italy
[25] INFN Sezione di Bologna, Bologna, Italy
[26] INFN Sezione di Ferrara, Ferrara, Italy
[27] INFN Sezione di Firenze, Firenze, Italy
[28] INFN Laboratori Nazionali di Frascati, Frascati, Italy
[29] INFN Sezione di Genova, Genova, Italy
[30] INFN Sezione di Milano, Milano, Italy
[31] INFN Sezione di Milano-Bicocca, Milano, Italy
[32] INFN Sezione di Cagliari, Monserrato, Italy
[33] INFN Sezione di Padova, Padova, Italy
[34] INFN Sezione di Perugia, Perugia, Italy
[35] INFN Sezione di Pisa, Pisa, Italy
[36] INFN Sezione di Roma La Sapienza, Roma, Italy
[37] INFN Sezione di Roma Tor Vergata, Roma, Italy
[38] Nikhef National Institute for Subatomic Physics, Amsterdam, Netherlands
[39] Nikhef National Institute for Subatomic Physics and VU University Amsterdam, Amsterdam, Netherlands
[40] AGH — University of Krakow, Faculty of Physics and Applied Computer Science, Kraków, Poland
[41] Henryk Niewodniczanski Institute of Nuclear Physics Polish Academy of Sciences, Kraków, Poland
[42] National Center for Nuclear Research (NCBJ), Warsaw, Poland
[43] Horia Hulubei National Institute of Physics and Nuclear Engineering, Bucharest-Magurele, Romania
[44] Authors affiliated with an institute formerly covered by a cooperation agreement with CERN.
[45] ICCUB, Universitat de Barcelona, Barcelona, Spain
[46] La Salle, Universitat Ramon Llull, Barcelona, Spain
[47] Instituto Galego de Física de Altas Enerxías (IGFAE), Universidade de Santiago de Compostela, Santiago de Compostela, Spain
[48] Instituto de Fisica Corpuscular, Centro Mixto Universidad de Valencia — CSIC, Valencia, Spain
[49] European Organization for Nuclear Research (CERN), Geneva, Switzerland
[50] Institute of Physics, Ecole Polytechnique Fédérale de Lausanne (EPFL), Lausanne, Switzerland
[51] Physik-Institut, Universität Zürich, Zürich, Switzerland
[52] NSC Kharkiv Institute of Physics and Technology (NSC KIPT), Kharkiv, Ukraine
[53] Institute for Nuclear Research of the National Academy of Sciences (KINR), Kyiv, Ukraine
[54] School of Physics and Astronomy, University of Birmingham, Birmingham, United Kingdom
[55] H.H. Wills Physics Laboratory, University of Bristol, Bristol, United Kingdom

JHEP07(2025)121

[56] Cavendish Laboratory, University of Cambridge, Cambridge, United Kingdom
[57] Department of Physics, University of Warwick, Coventry, United Kingdom
[58] STFC Rutherford Appleton Laboratory, Didcot, United Kingdom
[59] School of Physics and Astronomy, University of Edinburgh, Edinburgh, United Kingdom
[60] School of Physics and Astronomy, University of Glasgow, Glasgow, United Kingdom
[61] Oliver Lodge Laboratory, University of Liverpool, Liverpool, United Kingdom
[62] Imperial College London, London, United Kingdom
[63] Department of Physics and Astronomy, University of Manchester, Manchester, United Kingdom
[64] Department of Physics, University of Oxford, Oxford, United Kingdom
[65] Massachusetts Institute of Technology, Cambridge, MA, United States
[66] University of Cincinnati, Cincinnati, OH, United States
[67] University of Maryland, College Park, MD, United States
[68] Los Alamos National Laboratory (LANL), Los Alamos, NM, United States
[69] Syracuse University, Syracuse, NY, United States
[70] Pontifícia Universidade Católica do Rio de Janeiro (PUC-Rio), Rio de Janeiro, Brazil, associated to [3]
[71] School of Physics and Electronics, Hunan University, Changsha City, China, associated to [8]
[72] Guangdong Provincial Key Laboratory of Nuclear Science, Guangdong-Hong Kong Joint Laboratory of Quantum Matter, Institute of Quantum Matter, South China Normal University, Guangzhou, China, associated to [4]
[73] Lanzhou University, Lanzhou, China, associated to [5]
[74] School of Physics and Technology, Wuhan University, Wuhan, China, associated to [4]
[75] Henan Normal University, Xinxiang, China, associated to [8]
[76] Departamento de Fisica, Universidad Nacional de Colombia, Bogota, Colombia, associated to [16]
[77] Ruhr Universitaet Bochum, Fakultaet f. Physik und Astronomie, Bochum, Germany, associated to [19]
[78] Eotvos Lorand University, Budapest, Hungary, associated to [49]
[79] Faculty of Physics, Vilnius University, Vilnius, Lithuania, associated to [20]
[80] Van Swinderen Institute, University of Groningen, Groningen, Netherlands, associated to [38]
[81] Universiteit Maastricht, Maastricht, Netherlands, associated to [38]
[82] Tadeusz Kosciuszko Cracow University of Technology, Cracow, Poland, associated to [41]
[83] Universidade da Coruña, A Coruña, Spain, associated to [46]
[84] Department of Physics and Astronomy, Uppsala University, Uppsala, Sweden, associated to [60]
[85] Taras Schevchenko University of Kyiv, Faculty of Physics, Kyiv, Ukraine, associated to [14]
[86] University of Michigan, Ann Arbor, MI, United States, associated to [69]
[87] Ohio State University, Columbus, United States, associated to [68]

[a] Centro Federal de Educacão Tecnológica Celso Suckow da Fonseca, Rio De Janeiro, Brazil
[b] Center for High Energy Physics, Tsinghua University, Beijing, China
[c] Hangzhou Institute for Advanced Study, UCAS, Hangzhou, China
[d] LIP6, Sorbonne Université, Paris, France
[e] Lamarr Institute for Machine Learning and Artificial Intelligence, Dortmund, Germany
[f] Universidad Nacional Autónoma de Honduras, Tegucigalpa, Honduras
[g] Università di Bari, Bari, Italy
[h] Università di Bergamo, Bergamo, Italy
[i] Università di Bologna, Bologna, Italy
[j] Università di Cagliari, Cagliari, Italy
[k] Università di Ferrara, Ferrara, Italy
[l] Università di Firenze, Firenze, Italy
[m] Università di Genova, Genova, Italy
[n] Università degli Studi di Milano, Milano, Italy
[o] Università degli Studi di Milano-Bicocca, Milano, Italy
[p] Università di Padova, Padova, Italy
[q] Università di Perugia, Perugia, Italy
[r] Scuola Normale Superiore, Pisa, Italy
[s] Università di Pisa, Pisa, Italy

JHEP07(2025)121

[t] Università della Basilicata, Potenza, Italy
[u] Università di Roma Tor Vergata, Roma, Italy
[v] Università di Siena, Siena, Italy
[w] Università di Urbino, Urbino, Italy
[x] Universidad de Ingeniería y Tecnología (UTEC), Lima, Peru
[y] Universidad de Alcalá, Alcalá de Henares, Spain
[z] Facultad de Ciencias Fisicas, Madrid, Spain
[†] Deceased

JHEP07(2025)121